High-Speed and High-Resolution Interrogation of a Silicon Photonic Microdisk Sensor Based on Microwave Photonic Filtering

Hong Deng, *Student Member, IEEE*, Weifeng Zhang, *Student Member, IEEE*, and Jianping Yao ⓘ, *Fellow, IEEE, Fellow, OSA*

Abstract—High-speed and high-resolution interrogation of a silicon photonic microdisk sensor based on microwave photonic filtering and advanced signal processing is proposed and experimentally demonstrated. An integrated microdisk resonator (MDR) with a high Q factor is used as a sensor which is interrogated by incorporating the MDR into a microwave photonic filter (MPF) consisting of a laser source, a phase modulator (PM), the MDR, and a photodetector (PD), with the central frequency of the MPF being a function of the resonant wavelength of the MDR. A broadband linearly chirped microwave waveform (LCMW) is applied to the input of the MPF to generate a filtered microwave waveform. By measuring the temporal location of the filtered microwave waveform, the sensing information is revealed. To increase the signal-to-noise ratio (SNR) of the filtered microwave waveform, a phase-only filter (POF) realized based on the LCMW is correlated with the filtered microwave waveform, to generate a compressed pulse, which is filtered using a Hamming window to remove the noise and recorrelated with the POF to recover the filtered microwave waveform. Since the SNR is significantly increased, the interrogation accuracy is improved. The use of the proposed sensor for temperature and refractive index (RI) sensing is performed. The experimental results show that the sensor has a sensitivity of 76.8 pm/°C and a resolution of 0.234 °C as a temperature sensor, and a sensitivity of 33.28 nm/RIU and a resolution of 1.32×10^{-3} RIU as an RI sensor. The interrogation speed is as high as 100 kHz.

Index Terms—Microdisk resonator, microwave photonics, refractive index sensing, sensors, silicon photonics.

I. INTRODUCTION

FIBER optic sensors with advantageous features such as small size, low cost, immunity to electromagnetic interference (EMI), and high tolerance to harsh environment, have been extensively investigated in the last few years [1]. Numerous fiber-optic sensors based on a fiber Bragg grating (FBG) or an FBG array [2], a long period grating (LPG) [3], a nonlinear fiber [4]–[6], or an optical interferometer [7], [8] have been proposed.

These sensors are suitable for distributed strain and temperature sensing. However, for refractive index (RI) sensing or biosensing, optical fibers are too bulky to be sensitive to RI change or additional fiber processing has to be employed to increase the sensitivity [9]. On the other hand, thanks to the existing of an evanescent field around a silicon waveguide which can be altered with environmental changes, a sensor based on a silicon photonic waveguide has a high sensitivity to RI change. In addition, thanks to the ultra-small footprint, hundreds or even thousands of silicon photonic sensors can be integrated on a single chip, which can find applications in point-of-care testing (POCT) and other medical sensing [10], where multiple sensors are needed.

Silicon photonic resonators, such as waveguide Bragg gratings [11], phase-shifted Bragg gratings [12], microring resonators (MRRs) [13], and microdisk resonators (MDRs) [14], have been proposed and developed for sensing applications. Compared with a simple straight waveguide, the degree of interaction between the environment and the light field in a resonator sensor is enhanced by the number of roundtrips of the light inside the cavity, resulting in an increased sensitivity. The number of roundtrips is determined by the quality factor (Q factor) of a resonator. Thus, to get a higher sensitivity, a higher Q factor is needed [15]. On the other hand, a resonator with a higher Q factor will have a smaller 3-dB bandwidth. If interrogated by an optical spectrum analyzer (OSA), the interrogation speed is limited, especially for high-resolution interrogation.

Recently, optical sensors interrogated based on microwave photonics (MWP) techniques have been proposed [16]–[18]. By translating the wavelength shift in the optical domain to a microwave frequency change in the electrical domain and measuring the microwave frequency using a digital signal processor (DSP), the interrogation speed and resolution can be significantly increased [19]. An MRR-based sensor interrogated based on an optoelectronic oscillator (OEO) has recently been proposed. A detection sensitivity of 7.7 GHz/°C and a measurement resolution of 0.02 °C were achieved [20]. However, because of a large 3-dB bandwidth of the MRR, which is 1.75 GHz as reported in [20], the OEO loop must be very short and the gain in the loop must be precisely controlled to avoid mode hopping, to ensure stable oscillation, to make the frequency measurement accurate. In addition, an MRR-based sensor is

not suitable for biosensing, since the bandwidth of the MRR would be significantly broadened when the ring waveguide is cladded by a solution such as water or blood. Then, stable and single-frequency oscillation will be no longer maintained.

In this paper, an approach to achieve high speed and high resolution interrogation of a silicon photonic MDR sensor based on microwave photonic filtering is proposed and experimentally demonstrated. In the proposed system, the MDR is incorporated into a microwave photonic filter (MPF) consisting of a laser source, a phase modulator (PM), the MDR, and a photodetector (PD), with the central frequency of the MPF being a function of the resonant wavelength of the MDR. A broadband linearly chirped microwave waveform (LCMW) is applied to the input of the MPF to generate a filtered microwave waveform. By measuring the temporal location of the filtered microwave waveform, the sensing information is revealed. The interrogation resolution is determined by the bandwidth of the MDR. In the design, to get a high Q factor, the MDR is designed by adding a slab waveguide surrounding the disk and the bus waveguide, then the interaction between the light field and the sidewalls of the disk is weakened, thus the loss due to scattering resulted from sidewall roughness is suppressed and a higher Q factor is archived [21], which leads to an improved sensing sensitivity and interrogation resolution. The central frequency of the MPF is a function of the resonant wavelength of the MDR, which is sensitive to the change of the temperature or the cladding RI. To improve the signal-to-noise ratio (SNR) of the filtered microwave waveform, the microwave waveform is first compressed by correlating it with a phase-only filter (POF) built from the LCMW, which is a reference waveform. Then, a Hamming window is applied to the compressed pulse to remove the noise. By re-correlating the compressed waveform with the POF, a noise-removed microwave waveform is obtained, which is used to accurately estimate its temporal location. The use of the proposed sensor and it interrogation system for temperature and RI sensing is performed. The experimental results show that the sensor has a sensitivity of 76.8 pm/°C and a resolution of 0.234 °C as a temperature sensor, and a sensitivity of 33.28 nm/RIU and a resolution of 1.32×10^{-3} RIU as an RI sensor. The interrogation speed is as high as 100 kHz.

II. PRINCIPLE

Fig. 1(a) shows the configuration of the proposed interrogation system for temperature and RI sensing using a silicon photonic MDR sensor. It consists of a laser diode (LD), two polarization controllers (PC1 and PC2), a PM, an MDR, and a PD. A light wave generated by the LD is sent to the PM. The polarization direction of the incident light wave is aligned with the principle axis of the PM by PC1. The phase-modulated signal at the output of the PM is introduced to the on-chip MDR via PC2, which is used to ensure only the TE mode is excited in the waveguide. By filtering out one sideband of the phase-modulated signal by the notch of the MDR, phase modulation to intensity modulation (PM-IM) conversion is performed, and a microwave signal is recovered at the PD [22]. The overall operation is equivalent to an MPF with the center frequency of the
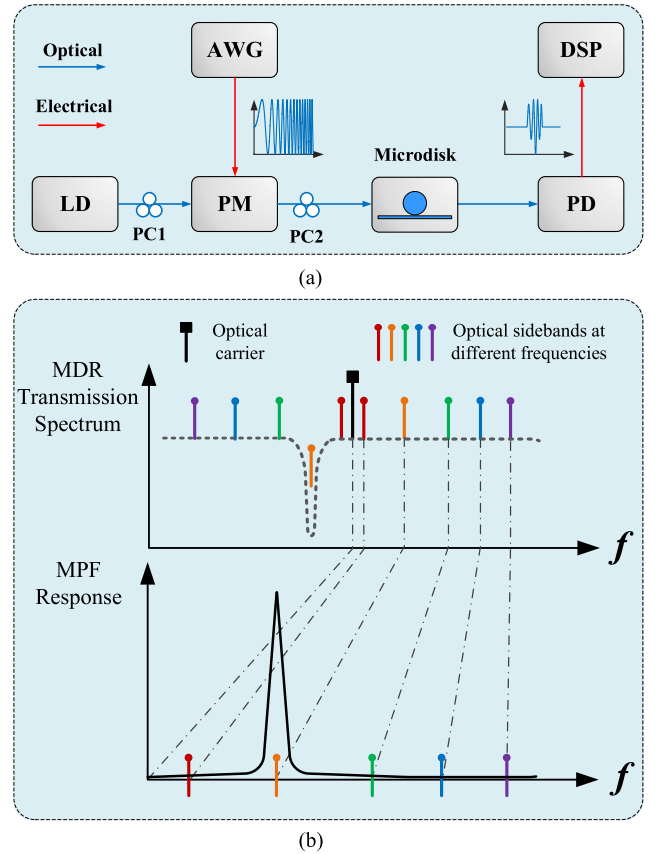

Fig. 1. (a) The configuration of the proposed interrogation system; (b) An MPF based on phase modulation to intensity modulation conversion. LD: laser diode; PC: polarization controller; PM: phase modulator; PD: photo detector; AWG: arbitrary waveform generator; DSP: digital signal processor.

passband equal to the wavelength difference between the optical carrier and the resonant wavelength of the MDR, as shown in Fig. 1(b). A broadband LCMW generated by an arbitrary waveform generator (AWG) is fed to the MPF. At the output of the MPF, a filtered microwave waveform with the central frequency determined by the passband of the MPF is obtained. The location of the filtered microwave waveform is determined by the central frequency of the MPF, thus by estimating the temporal location of the filtered microwave waveform, the wavelength shift of the MDR is obtained, which is an indicator of the temperature or RI change.

The resonant wavelength of an MDR can be expressed as [23]

$$\lambda_{res} = \frac{2\pi R}{m} n_{eff} \qquad (1)$$

where R is the disk radius, m is the mode order and n_{eff} is the effective index of the guided mode in the waveguide. When the environmental temperature changes, the effective index will change due to the thermos-optic effect, and the radius will also change due to the thermal expansion effect. So, the overall wavelength shift is given by [24]

$$\Delta\lambda_{Temp} = \frac{\lambda_{res}}{n_g} \Delta T \left(\alpha_{si} n_{eff} + \frac{\partial n_{eff}}{\partial T} \right) \qquad (2)$$

where n_g is the group index of the guided mode, ΔT is the temperature change, α_{si} is the thermal expansion coefficient and $\partial n_{eff}/\partial T$ is the thermos-optic coefficient.

When the RI of the cladding (n_{clad}) changes, the effective index of the guided mode will also change, leading to a resonant wavelength shift, which is given by [25]

$$\Delta\lambda_{RI} = \left(\frac{\lambda_{res}}{n_g}\right) \times \Delta n_{clad} \times \left(\frac{\partial n_{eff}}{\partial n_{clad}}\right) \tag{3}$$

where Δn_{clad} is the cladding RI change.

Assuming the wavelength of the optical carrier is λ_c, the central frequency of the MPF is given by

$$f_{MPF} \approx \left(\frac{c}{n_{avg}}\right) \times \left|\frac{\lambda_c - \lambda_{res}}{\lambda_c^2}\right| \tag{4}$$

where c is the velocity of light in vacuum, n_{avg} is the average refractive index for the optical path consisting of fibers and the silicon waveguides. When the resonate wavelength of the MDR shifts, the central frequency of the MPF will change. The frequency change can be expressed as

$$\Delta f_{MPF} = K\Delta\lambda_{res} \tag{5}$$

where $K = c/(n\lambda_c^2)$ and $\Delta\lambda_{res}$ is the wavelength shift ($\Delta\lambda_{Temp}$ and $\Delta\lambda_{RI}$).

Mathematically, for a LCMW, the instantaneous frequency of the waveform is given by

$$f(t) = f_0 + Ct \tag{6}$$

where C is the chirp rate, f_0 is the initial frequency, and t is the time. When a LCMW is fed to an MPF, the temporal location of the output waveform is calculated by $t = (f_{MPF} - f_0)/C$. The relationship between the wavelength shift of the MDR and the temporal location is given by

$$\Delta t = \frac{K}{C}\Delta\lambda_{res} \tag{7}$$

When the temporal location is measured, using (7) with (2) or (3), the temperature or the RI change can be calculated.

The interrogation resolution is limited by the 3-dB bandwidth of the MPF, which determines the spectral width of the filtered microwave waveform. To reduce the bandwidth of the MPF, the Q factor of the MDR should be increased. To do so, we add a slab waveguide surrounding the disk and the bus waveguide, to reduce the loss due to sidewall roughness [21]. The 3D view and the cross-sectional view of the MDR are shown in Fig. 2(a). The radius of the microdisk is 3.7 μm, and the width of the bus waveguide is 520 nm. A slab waveguide with a height of 60 nm is added surrounding the disk and the bus waveguides. To increase the sensitivity, a direct contact between the MDR sensor and a solution for which its RI is to be measured is needed [26]. To do so, the silica cladding is removed. Fig. 2(b) shows the simulated fundamental mode profile in a conventional MDR, and Fig. 2(c) shows the fundamental mode profile in the proposed MDR. Comparing the two mode profiles, it can be clearly seen that the interaction between the light field and the sidewalls of the proposed MDR is weakened. Thus, the scattering due to sidewall roughness is reduced and a higher Q factor is ensured.
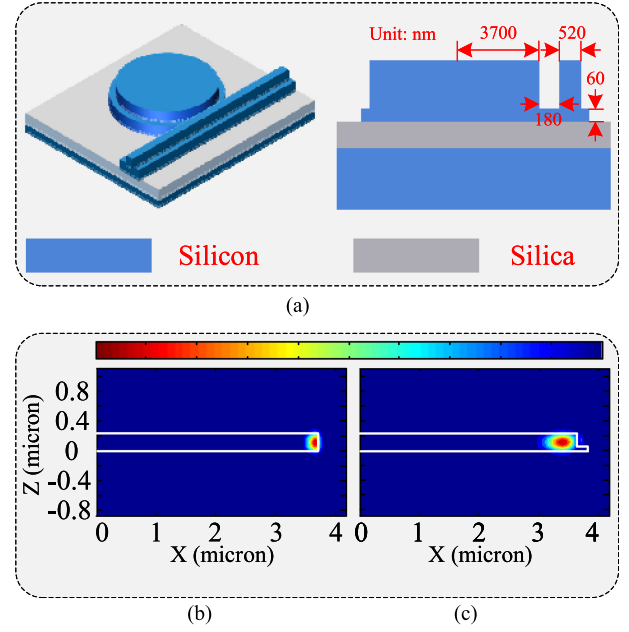

Fig. 2. (a) 3-D view and cross-sectional view of the proposed MDR; (b) simulated fundamental TE$_0$ profile of a conventional MDR; (c) simulated fundamental TE$_0$ profile of the proposed MDR.
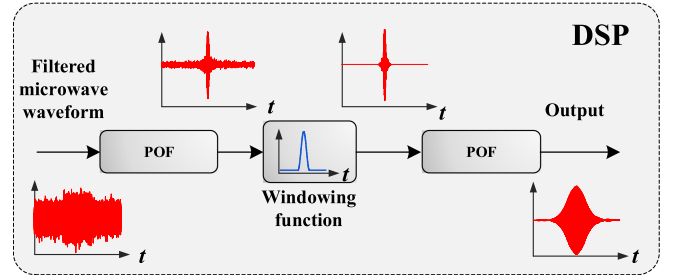

Fig. 3. Signal processing to improve the SNR of the filtered microwave waveform.

The detection accuracy is affected by the noise of the filtered microwave waveform [15]. Due to a high insertion loss of the system, the filtered microwave waveform is weak with a poor SNR. To increase the SNR to ensure an accurate measurement of the time shift, the filtered microwave waveform is filtered using a DSP. The signal processing procedure is shown in Fig. 3. A POF based on the reference LCMW is built which is correlated with the filtered microwave waveform, thus the microwave waveform is compressed. On the other hand, since the noise is not correlated with the LCMW, its distribution after phase-only filtering is not changed. Thus, by applying a windowing function to select the compressed pulse, the noise is significantly suppressed. Finally, by re-correlating the noise-suppressed compressed pulse with the POF, a microwave waveform with an increased SNR is obtained.

Mathematically, the filtered microwave waveform at the output of the PD can be expressed as

$$x(t) = s(t) + n(t) \tag{8}$$

where $s(t)$ is the filtered microwave waveform and $n(t)$ is the noise.

We use the LCMW, denoted as $r(t)$, generated by the AWG, as a reference to build a POF. Considering the spectrum of the reference $R(j\omega)$, the spectrum response of the POF is $\frac{R(j\omega)}{|R(j\omega)|}$. The compressed pulse is given by

$$Y_1(t) = F^{-1}\left[X(j\omega) \times \frac{R^*j(\omega)}{|R(j\omega)|}\right]$$

$$= F^{-1}\left\{[S(j\omega) + N(j\omega)] \times e^{-j\phi_R(j\omega)}\right\}$$

$$= F^{-1}\Big[|S(j\omega)|e^{j\phi_s(j\omega)} \times e^{-j\phi_R(j\omega)}$$

$$+ |N(\omega)|e^{j\phi_n(j\omega)}e^{-j\phi(j\omega)}\Big] \qquad (9)$$

where $R^*(j\omega)$ is the complex conjugate of $R(j\omega)$, $X(j\omega)$, $S(j\omega)$ and $N(j\omega)$ are the Fourier transforms of $x(t)$, $s(t)$ and $n(t)$, respectively, and $\phi_s(j\omega)$, $\phi_n(j\omega)$ and $\phi_R(j\omega)$ are the phase terms of $S(j\omega)$, $N(j\omega)$ and $R(j\omega)$, respectively.

Because the filtered microwave waveform is from the reference LCMW and the MPF has a linear phase response, we have $\phi_s(j\omega) = \phi_R(j\omega)$. Thus, (9) is simplified to be

$$Y_1(t) = F^{-1}\left[|S(j\omega)| + |N(j\omega)|e^{j\phi_n(j\omega)}e^{-j\phi_R(j\omega)}\right] \quad (10)$$

From (10), we can see that the filtered microwave waveform is compressed. On the other hand, since the phase term of the noise is randomly distributed, it is not cancelled by the phase term of the POF during the correlation process, thus the noise is still uniformly distributed and no compression is imposed to the noise. By applying a windowing function to select the compressed pulse, the noise would be significantly suppressed. Then, by re-correlating the compressed pulse with the POF, the microwave waveform is recovered, but with a significantly increased SNR.

$$Y_2(t) = F^{-1}\bigg[\Big(|S(j\omega)| + |N'(j\omega)|e^{j\phi_n(j\omega)}e^{-j\phi_R(j\omega)}\Big)$$

$$\times \frac{R^*(j\omega)}{|R(j\omega)|}\bigg]$$

$$= F^{-1}\Big[|S(j\omega)|e^{-j\phi_R(j\omega)}$$

$$+ |N'(j\omega)|e^{j\phi_n(j\omega)}e^{-j2\phi_R(j\omega)}\Big] \qquad (11)$$

where $N'(\omega)$ is the spectrum of the noise after windowing.

From (11), it can be seen that the microwave waveform after signal processing is a time reversed version of the microwave waveform at the output of the PD, but the noise is significantly suppressed. Thus, the filtered microwave waveform is rebuilt with an improved SNR.

The bandwidth of the filtered microwave waveform is determined by the bandwidth of the MDR, given by

$$B = K\frac{\lambda_{res}}{Q} \qquad (12)$$

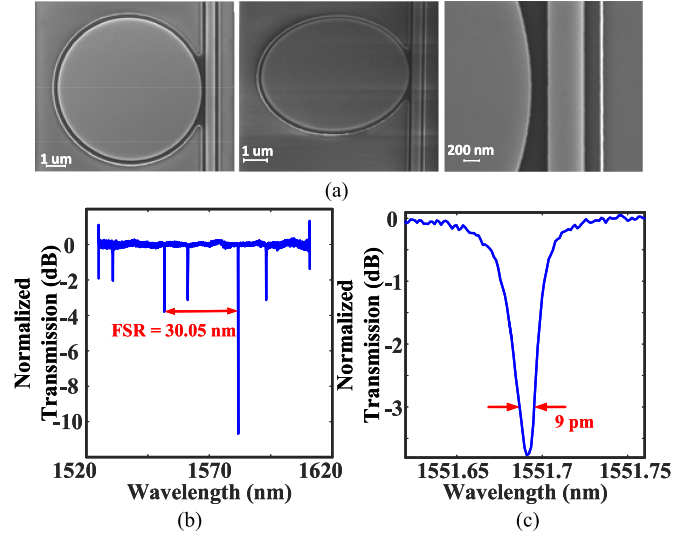where Q is the quality factor and $K = c/(n\lambda_c^2)$.

Fig. 4. (a) SEM micrographs of the fabricated MDR (with the left picture taken vertically, the middle taken with a tilted angle of 45°, and the right showing the zoom-in view of the gap); (b) normalized transmission spectrum of the fabricated MDR with air cladding; (c) zoom-in view of the TE$_0$ mode resonance of the fabricated MDR with air cladding.

The time bandwidth product (TBWP) of the filtered microwave waveform is

$$TBWP = \frac{K^2\lambda_{res}^2}{Q^2C} \qquad (13)$$

At the output of the first POF, the temporal duration of the filtered microwave waveform is compressed by TBWP times. Since the noise after the POF is still uniformly distributed, if a Hamming window with a 3-dB bandwidth equal to the width of the compressed waveform is applied, the microwave waveform is not affected, but the noise is significantly reduced by TBWP times. Thus, the SNR of the filtered microwave waveform is increased by $10\log_{10}(TBWP)$ dB. For example, if the TBWP is 1,000, the SNR is increased by 30 dB.

III. EXPERIMENT

An experiment based on the setup shown in Fig. 1(a) is performed. A CW light from a tunable laser source (TLS) (Anritsu, MG9638A) is sent to the PM (Thorlabs, 40 GHz) via PC1, where it is phase modulated by a broadband LCMW, generated by an AWG (Keysight M8195A). Then, the modulated light wave is introduced to the MDR, where the 1st order sideband is eliminated and PM-IM conversion is performed. At the output of the MDR, the optical carrier and the other 1st order sideband are sent to the PD (Newport, model 1014, 45 GHz). A filtered microwave waveform is generated at the output of the PD, which is sent to a DSP for signal processing.

The key device in the system is the silicon photonic MDR, which is fabricated using CMOS-compatible technology with 193-nm optical projection lithography [21]. Fig. 4(a) shows the SEM micrographs of the fabricated MDR. An optical vector analyzer (OVA, LUNA OVA 5000) is used to evaluate the optical performance. Fig. 4(b) shows the spectral response of the MDR, and Fig. 4(c) gives a zoom-in view of a TE0 mode
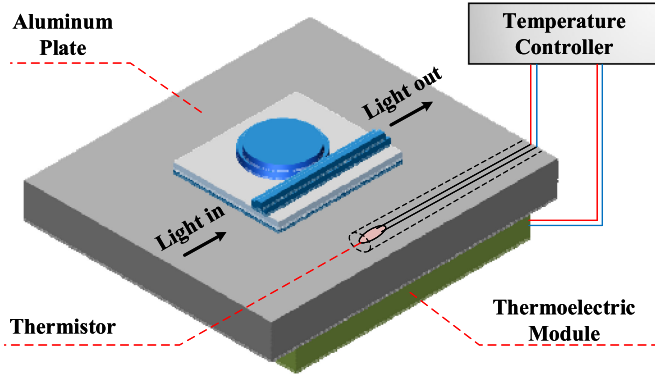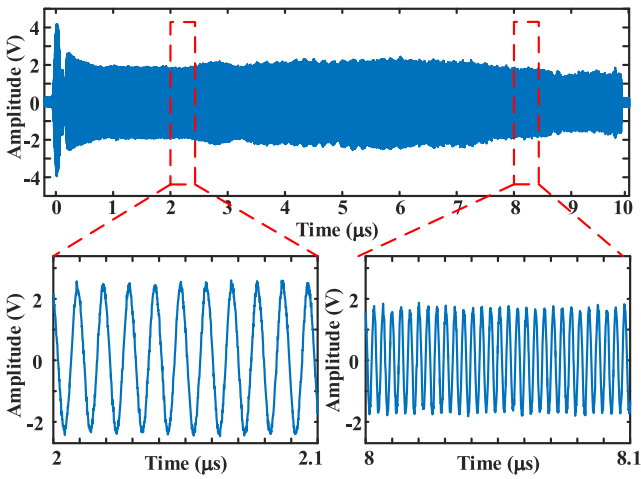
Fig. 5. The schematic of the setup for thermal control.

Fig. 6. Broadband LCMW generated by an AWG. Two inserts show the temporal waveforms at the lower and higher frequency regions.
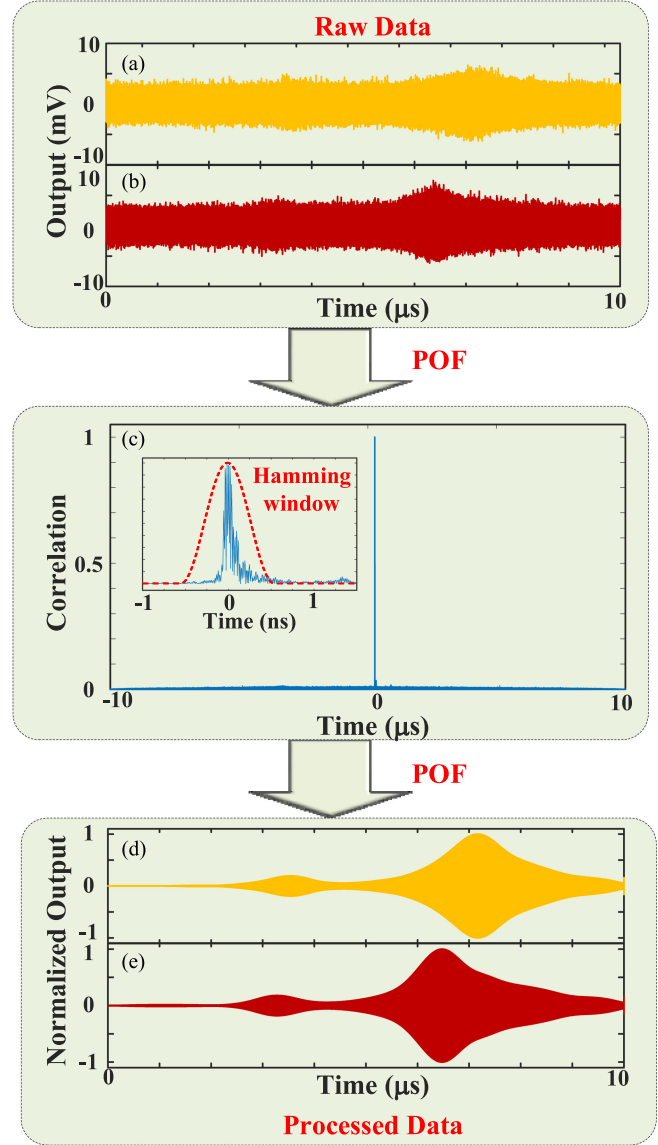

Fig. 7. (a) Generated filtered microwave waveform at 22.82 °C; (b) generated filtered microwave waveform at 23.03 °C; (c) the normalized cross-correlation result. The red dash line in the zoom-in insert shows the applied Hamming window; (d) the recovered microwave waveforms corresponding to the filtered microwave waveforms at 22.82 °C shown in (a); (e) the recovered microwave waveform corresponding to the filtered microwave waveform at 23.03 °C shown in (b).

resonance. As can be seen, the free spectral range (FSR) of the MDR is 30.05 nm, and the 3-dB bandwidth is around 9 pm (or 1.125 GHz). The Q factor of the fabricated MDR is calculated to be 172,400, which is much greater than a conventional MDR [14], thus an improved interrogation resolution is ensured.

Firstly, the resonant wavelength shift with the temperature change is investigated. The schematic of the setup for thermal control is shown in Fig. 5. A temperature controller (ILX Lightwave, LDT-5910B) with a thermoelectric module and a thermistor is used to control the temperature of the chip, which can provide a temperature resolution of ± 0.1 °C. The wavelength of the optical carrier is set at 1552.27 nm, and an LCMW with a temporal duration of 10 μs and a chirp rate of 3.2 GHz/μs is generated by the AWG as the modulation signal, which is shown in Fig. 6. Fig. 7(a) and (b) shows two filtered microwave waveforms at two different temperature levels at the output of the PD. As can be seen, the filtered microwave waveforms are separated in the time domain, with the temporal separation corresponding to the wavelength change of the MDR. The temporal width of a filtered microwave waveform is around 700 ns. Since the microwave waveforms are very noisy, an accurate estimation of the temporal locations of the filtered microwave waveforms is difficult. A solution is to filter out the noise, which can be performed

by phase-only filtering to compress the waveforms, followed by windowing to remove the noise, and then a second, but identical phase-only filtering to recover the filtered microwave waveform, all are done in a DSP. Fig. 7(c) shows a compressed microwave pulse which is obtained by correlating the filtered microwave waveform with a POF built from the LCMW. Thanks to the large TBWP of the filtered microwave waveform, the width of the compressed pulse after the POF is only around 0.4 ns, with a compression ratio of around 1,758. By applying a Hamming window to the compressed pulse with a width of 0.7 ns to remove the noise and feeding the noise-removed compressed pulse to the POF again, the microwave waveform is recovered and the noise is significantly attenuated.
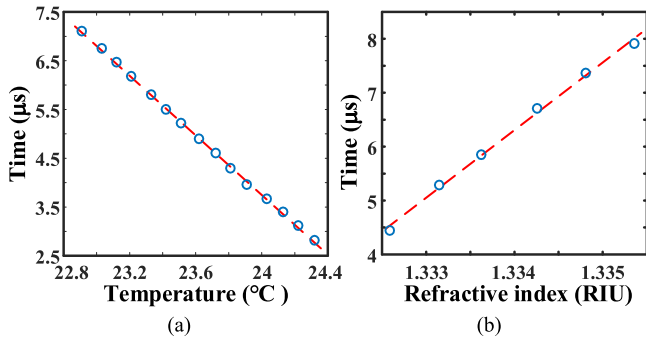
Fig. 8.   Experimental results. (a) Temporal locations vs. temperature change; (b) temporal locations vs. cladding RI change. The circles are the experimental data, and the red-dash lines show the linear fitting of the experimental data.
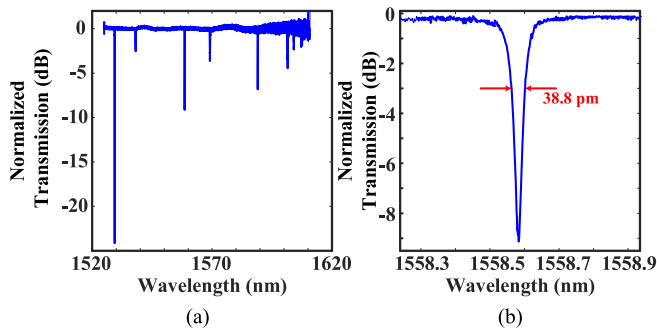

Fig. 9.   (a) Normalized transmission spectrum of the fabricated MDR with water cladding; (b) zoom-in view of the TE_0 mode resonance of the fabricated MDR with water cladding.

Fig. 7(d) and (e) shows the processed waveforms corresponding to those waveforms shown in Fig. 7(a) and (b), respectively. Since the noise is significantly suppressed, the temporal locations of the microwave waveforms can be accurately estimated. Fig. 8(a) shows estimated temporal locations vs. temperature change. As can be seen the sensitivity for temperature measurement is 3.07 μs/°C, or 76.8 pm/°C. Because of the nonlinear optical phase response of the MDR which would broaden the bandwidth of the MPF, the measured 3-dB bandwidth of the MPF is 2.25 GHz, which is larger than the bandwidth of the MDR (9 pm or 1.125 GHz). The corresponding sensing resolution is 0.234 °C.

Then, the resonant wavelength shift with the RI change is investigated. Setting a temperature at 23.4 °C and the wavelength of the light carrier at 1558.35 nm, we change the cladding RI by changing the RI of the NaCl solution. The RI of the NaCl solution is measured by a refractometer. Fig. 8(b) shows the estimated temporal locations vs. the cladding RI change. From the fitted line, it can be seen that the sensitivity for RI measurement is 1.3 ms/RIU, or 33.28 nm/RIU.

Note that when the MDR is cladded with a NaCl solution, the Q factor of the MDR is reduced and the bandwidth is broadened. In the experiment, the measured 3-dB bandwidth of the MPF is 5.5 GHz, corresponding to a sensing resolution of 1.32×10^{-3} RIU.

Note also that the change of the cladding RI of the cladding is significant, the resonant wavelength has a large shift. As shown in Fig. 9(a), when the MDR is cladded with water, the resonant wavelength is shifted to 1558.59 nm, a net shift of 6.99 nm. From the zoom-in view shown in Fig. 9(b), it can be noticed that the 3-dB bandwidth is increased to around 39 pm and the Q factor is reduced to 40,000, which is due to the change in coupling coefficient between the bus and the microdisk.

IV. CONCLUSION

High-speed and high-resolution interrogation of a silicon photonic MDR sensor based on microwave photonic filtering with improved sensing resolution and speed was proposed and experimentally demonstrated. To get a high sensing resolution, a high Q factor MDR by adding a slab waveguide surrounding the waveguide bus and the microdisk was designed and fabricated and its use for temperature and RI sensing was performed. To increase interrogation speed, the wavelength change of the MDR was converted to the temporal location change of a filtered microwave waveform, which was generated by filtering a broadband LCMW using an MPF. Since the interrogation can be performed in the electrical domain using a DSP, the speed was significantly increased. To increase the interrogation accuracy, the noise of the filtered microwave waveform was removed by an advanced signal processing approach in which two phase-only filtering operations were performed. By using a Hamming window to select the compressed waveform after the first phase-only filtering, the noise was significantly reduced. The interrogation speed of this system was determined by the temporal duration of the LCMW, which was 10 μs, corresponding an interrogation speed of 100 kHz. The proposed sensor system was experimentally demonstrated. As a temperature sensor, a sensitivity of 76.8 pm/°C and a resolution of 0.234 °C were achieved. As an RI sensor, a sensitivity of 33.28 nm/RIU and a resolution of 1.32×10^{-3} RIU were achieved.

REFERENCES

[1] S. Yin, P Ruffin, and F. Yu, *Fiber Optic Sensors*, 2nd ed. Boca Raton, FL, USA: CRC Press, 2008.
[2] A. D. Kersey, T. A. Berkoff, and W. W. Morey, "Multiplexed fiber Bragg grating strain-sensor system with a fiber Fabry–Perot wavelength filter," *Opt. Lett.*, vol. 18, no. 16, pp. 1370–1372, Aug. 1993.
[3] H. J. Patrick, G. M. Williams, A. D. Kersey, J. R. Pedrazzani, and A. M. Vengsarkar, "Hybrid fiber Bragg grating/long period fiber grating sensor for strain/temperature discrimination," *IEEE Photon. Technol. Lett.*, vol. 8, no. 9, pp. 1223–1225, Sep. 1996.
[4] M. Niklès, L. Thévenaz, and P. A. Robert, "Simple distributed fiber sensor based on Brillouin gain spectrum analysis," *Opt. Lett.*, vol. 21, no. 10, pp. 758–760, May 1996.
[5] M. G. Tanner, S. D. Dyer, B. Baek, R. H. Hadfield, and S. W. Nam, "High-resolution single-mode fiber-optic distributed Raman sensor for absolute temperature measurement using superconducting nanowire single-photon detectors," *Appl. Phys. Lett.*, vol. 99, no. 20, Nov. 2011, Art. no. 201110.
[6] R. A. Bergh, H. C. Lefevre, and H. J. Shaw, "Compensation of the optical Kerr effect in fiber-optic gyroscopes," *Opt. Lett.*, vol. 7, no. 6, pp. 282–284, Jun. 1982.
[7] Z. Tian *et al.*, "Refractive index sensing with Mach–Zehnder interferometer based on concatenating two single-mode fiber tapers," *IEEE Photon. Technol. Lett.*, vol. 20, no. 8, pp. 626–628, Apr. 2008.
[8] Z. Tian, S. H. Yam, and H. P. Loock, "Refractive index sensor based on an abrupt taper Michelson interferometer in a single-mode fiber," *Opt. Lett.*, vol. 33, no. 10, pp. 1105–1107, May 2008.
[9] A. D. Kersey *et al.*, "Fiber grating sensors," *J. Lightw. Technol.*, vol. 15, no. 8, pp. 1442–1463, Aug. 1997.
[10] R. Soref, "The past, present, and future of silicon photonics," *IEEE J. Sel. Topics Quantum Electron.*, vol. 12, no. 6, pp. 1678–1687, Nov. 2006.

[11] I. Rea, M. Iodice, G. Coppola, I. Rendina, A. Marino, and L. D. Stefano, "A porous silicon-based Bragg grating waveguide sensor for chemical monitoring," *Sens Actuat. B Chem.*, vol. 139, no. 1, pp. 39–43, May 2009.

[12] P. Prabhathan, V. Murukeshan, Z. Jing, and P. Ramana, "Compact SOI nanowire refractive index sensor using phase shifted Bragg grating," *Opt. Exp.*, vol. 17, no. 17, pp. 15330–15341, Aug. 2009.

[13] K. D. Vos, I. Bartolozzi, E. Schacht, P. Bienstman, and R. Baets, "Silicon-on-Insulator microring resonator for sensitive and label-free biosensing," *Opt. Exp.*, vol. 15, no. 12, pp. 7610–7615, Jun. 2007.

[14] S. M. Grist *et al.*, "Silicon photonic micro-disk resonators for label-free biosensing," *Opt. Express*, vol. 21, no. 7, pp. 7994–8006, Apr. 2013.

[15] L. Chrostowski *et al.*, "Silicon photonic resonator sensors and devices," *Proc. SPIE*, vol. 8236, Feb. 2012, Art. no. 823620.

[16] W. Liu, W. Li, and J. P. Yao, "Real-time interrogation of a linearly chirped fiber Bragg grating sensor for simultaneous measurement of strain and temperature," *IEEE Photon. Technol. Lett.*, vol. 23, no. 18, pp. 1340–1342, Sep. 2011.

[17] O. Xu, J. Zhang, H. Deng, and J. P. Yao, "Dual-frequency optoelectronic oscillator for temperature-insensitive interrogation of a FBG sensor," *IEEE Photon. Technol. Lett.*, vol. 29, no. 4, pp. 357–360, Feb. 2017.

[18] J. P. Yao, "Optoelectronic oscillators for high speed and high resolution optical sensing," *IEEE/OSA J. Lightw. Technol.*, vol. 35, no. 16, pp. 3489–3497, Aug. 2017.

[19] J. P. Yao, "Microwave photonics for high resolution and high speed interrogation of fiber Bragg grating sensors," *Fiber Integr. Opt.*, vol. 34, no. 4, pp. 230–242, Oct. 2015.

[20] S. X. Chew *et al.*, "Optoelectronic oscillator based sensor using an on-chip sensing probe," *IEEE Photon. J.*, vol. 9, no. 2, pp. 1–9, Apr. 2017.

[21] W. Zhang and J. P. Yao, "Silicon-based on-chip microdisk resonators for integrated microwave photonic applications," in *Proc. Opt. Fiber Conf.*, Anaheim, CA, USA, Mar. 2016, Paper no. M2B.6.

[22] W. Li, M. Li, and J. P. Yao, "A narrow-passband and frequency-tunable micro-wave photonic filter based on phase-modulation to intensity-modulation conversion using a phase-shifted fiber Bragg grating," *IEEE Trans. Microw. Theory Techn.*, vol. 60, no. 5, pp. 1287–1296, May 2012.

[23] W. Bogaerts *et al.*, "Silicon microring resonators," *Laser Photon. Rev.*, vol. 6, no. 1, pp. 47–73, Sep. 2011.

[24] G. D. Kim *et al.*, "Silicon photonic temperature sensor employing a ring resonator manufactured using a standard CMOS process," *Opt. Exp.*, vol. 18, no. 21, pp. 22215–22221, Oct. 2010.

[25] J. J. Ackert *et al.*, "Defect-mediated resonance shift of silicon-on-insulator racetrack resonators," *Opt. Exp.*, vol. 19, no. 13, pp. 11969–11976, Jun. 2011.

[26] T. Yoshie, L. Tang, and S. Y. Su, "Optical microcavity: sensing down to single molecules and atoms," *Sensors*, vol. 11, no. 2, pp. 1972–1991, Feb. 2011.

Hong Deng (S'16) received the B.Eng. degree in optoelectronic information engineering from Huazhong University of Science and Technology, Wuhan, China, in 2014. He is currently working toward the master's degree at Microwave Photonics Research Laboratory, School of Electrical Engineering and Computer Science, University of Ottawa, Ottawa, ON, Canada. His current research interests include photonic generation of microwave waveforms, fiber optic sensors, and silicon photonics.

Weifeng Zhang (S'12) received the B.Eng. degree in electronic science and technology from Xi'an Jiaotong University, Xi'an, China, in 2008, the M.A.Sc. degree in electrical engineering from the Politecnico di Torino, Torino, Italy, in 2011, and the Ph.D. degree in electrical engineering from the University of Ottawa, Ottawa, ON, Canada. He is currently working as a Post-Doctor Fellow in Microwave Photonics Research Laboratory, School of Electrical Engineering and Computer Science, University of Ottawa. His current research interests include silicon photonics and its applications in microwave photonics.

Jianping Yao (M'99–SM'01–F'12) received the Ph.D. degree in electrical engineering from the Université de Toulon et du Var, France, in 1997. He is a Distinguished University Professor and University Research Chair in the School of Electrical Engineering and Computer Science, University of Ottawa, Ottawa, ON, Canada. From 1998 to 2001, he was with the School of Electrical and Electronic Engineering, Nanyang Technological University (NTU), Singapore, as an Assistant Professor. In December 2001, he joined the School of Electrical Engineering and Computer Science, University of Ottawa, as an Assistant Professor, where he was promoted to Associate Professor in May 2003, and Full Professor in May 2006. He was appointed the University Research Chair in Microwave Photonics in 2007. In June 2016, he was conferred the title of Distinguished University Professor of the University of Ottawa. From July 2007 to June 2010 and July 2013 to June 2016, he was the Director of the Ottawa-Carleton Institute for Electrical and Computer Engineering.

He has authored or coauthored more than 560 research papers including more than 330 papers in peer-reviewed journals and more than 230 papers in conference proceedings. He is Editor-in-Chief of IEEE PHOTONICS TECHNOLOGY LETTERS, a former Topical Editor of *Optics Letters*, an Associate Editor of *Science Bulletin*, a Steering Committee Member of IEEE JOURNAL OF LIGHTWAVE TECHNOLOGY, and an Advisory Editorial Board Member of *Optics Communications*. He was a Guest Editor of a Focus Issue on Microwave Photonics in *Optics Express* in 2013, a Lead-Editor of a Feature Issue on Microwave Photonics in *Photonics Research* in 2014, and a Guest Editor of a special issue on Microwave Photonics in IEEE/OSA JOURNAL OF LIGHTWAVE TECHNOLOGY in 2018. He currently serves as the Chair of the IEEE Photonics Ottawa Chapter, and is the Technical Committee Chair of IEEE MTT-3 Microwave Photonics. He was a Member of the European Research Council Consolidator Grant Panel in 2016, the Qualitative Evaluation Panel in 2017, and a Panelist of the National Science Foundation Career Awards Panel in 2016. He has also served as a Chair of a number of international conferences, symposia, and workshops, including the Vice Technical Program Committee (TPC) Chair of the 2007 IEEE Topical Meeting on Microwave Photonics, TPC Co-Chair of the 2009 and 2010 Asia-Pacific Microwave Photonics Conference, TPC Chair of the high-speed and broadband wireless technologies subcommittee of the IEEE Radio Wireless Symposium 2009-2012, TPC Chair of the microwave photonics subcommittee of the IEEE Photonics Society Annual Meeting 2009, TPC Chair of the 2010 IEEE Topical Meeting on Microwave Photonics, General Co-Chair of the 2011 IEEE Topical Meeting on Microwave Photonics, TPC Co-Chair of the 2014 IEEE Topical Meetings on Microwave Photonics, and General Co-Chair of the 2015 and 2017 IEEE Topical Meeting on Microwave Photonics. He also served as a committee member for a number of international conferences, such as IPC, OFC, BGPP and MWP. He received the 2005 International Creative Research Award of the University of Ottawa. He received the 2007 George S. Glinski Award for Excellence in Research. In 2008, he received the Natural Sciences and Engineering Research Council of Canada Discovery Accelerator Supplements Award. He was selected to receive an inaugural OSA Outstanding Reviewer Award in 2012 and was one of the top ten reviewers of IEEE/OSA JOURNAL OF LIGHTWAVE TECHNOLOGY 2015–2016. He was an IEEE MTT-S Distinguished Microwave Lecturer for 2013–2015. He received the 2017–2018 Award for Excellence in Research of the University of Ottawa, and the 2018 R.A. Fessenden Silver Medal from IEEE Canada. He is a registered Professional Engineer of Ontario. He is a Fellow of the Optical Society of America and the Canadian Academy of Engineering.